Landslides (2018) 15:1615–1630
DOI 10.1007/s10346-018-0972-6
Received: 25 September 2017
Accepted: 26 February 2018
Published online: 12 March 2018

S. R. Carrière · D. Jongmans · G. Chambon · G. Bièvre · B. Lanson · L. Bertello · M. Berti · M. Jaboyedoff · J.-P. Malet · J. E. Chambers

Rheological properties of clayey soils originating from flow-like landslides

Abstract Flow-like landslides in clayey soils represent serious threats for populations and infrastructures and have been the subject of numerous studies in the past decade. However, despite the rising need for landslide mitigation with growing urbanization, the transient mechanisms involved in the solid-fluid transition are still poorly understood. One way of characterizing the solid-fluid transition is to carry out rheometrical tests on clayey soil samples to assess the evolution of viscosity with the shear stress. In this study, we carried out geotechnical and rheometrical tests on clayey samples collected from six flow-like landslides in order to assess if these clayey soils exhibit similar characteristics when they fluidize (solid-fluid transition). The results show that (1) all tested soils except one exhibit a yield-stress fluid behavior that can be associated with a bifurcation in viscosity (described by the critical shear rate $\dot{\gamma}_c$) and in shear modulus G; (2) the larger the amplitude of the viscosity bifurcation, the larger the associated drop in G; and (3) the water content (w) deviation from the Atterberg liquid limit (LL) seem a key parameter controlling a common mechanical behavior of these soils at the solid-fluid transition. We propose exponential laws describing the evolution of the critical shear stress τ_c, the critical shear rate $\dot{\gamma}_c$, and the shear modulus G as a function of the deviation w-LL.

Keywords Clay · Solid-fluid transition · Rheology · Viscosity bifurcation · Atterberg limits

Introduction

Landslides in clay-rich soils are very common and exhibit a large variety of sizes, morphologies, and kinematics (Maquaire et al. 2003; Mackey et al. 2009; Picarelli et al. 2005, Chambers et al. 2011; Bièvre et al. 2011). Particularly intriguing are the complex processes through which initially rigid slides can transform into flow-type movements like mud flows or debris flows (van Asch and Malet 2009; Mainsant et al. 2012a). Slow-moving earthflows, with typical velocities of meters per year (m year^{-1}), can suddenly accelerate and acquire velocities ranging from meters per hour (m h^{-1}) to meters per second (m s^{-1}) (Hungr et al. 2014). These apparently unpredictable acceleration and fluidization events constitute a serious threat to local populations and infrastructures. Although the triggering mechanisms always appear to involve a rapid increase in soil water content, generally caused by heavy and/or long-lasting rainfalls, the current ability to forecast and model these events is still limited. In geotechnics, the mechanical behavior of cohesive soils is classically characterized by two experimentally determined water contents, the Atterberg plastic and liquid limits PL and LL (Mitchell 1993). A fair assumption is then to consider that fluidization of the moving mass, and slide-to-flow transition, occur when the water content w reaches the liquid limit LL (e.g., Hungr et al. 2014). However, this interpretation disregards the stress state within the material, which constitutes the driving force of the instability. One of the main challenges therefore lies in the characterization of the mechanical behavior (stress–strain–shear rate relations) of these clayey landslides in the vicinity of the apparent solid-fluid transition.

From a mechanical point of view, two main approaches coexist to describe the generation of mud and debris flows from landslides. The *two-phase* approach posits that solid-fluid transition is caused by an increase in interstitial pore pressure, i.e. by a decrease in effective normal stresses in the soil (e.g., Iverson 1997, 2005; Iverson and George 2016; Picarelli et al. 2004). The rheological approach, on the other hand, assumes that the material can be described by an effective single-phase constitutive law, and that fluidization occurs when a critical stress threshold is exceeded (Ancey 2007; Mainsant et al. 2015). While the former approach is well suited to frictional materials, whose strength is intrinsically pressure-dependent, the latter better applies to cohesive materials with high water content ($w \approx LL$), for which strength can be regarded, at least as a first approximation, as an intrinsic rheological property (Coussot and Piau 1994; Coussot and Ancey 1999). The present study takes place within the rheological framework and investigates the possibility to describe solid-fluid transition in clayey landslides in terms of a few characteristic rheological parameters. Following the most recent landslide classification proposed by Hungr et al. (2014), we consider here clay soils as soils with a plasticity index $PI = LL$-PL larger than 5%. The cohesive character of these soils arises from the relatively large proportion of fine particles (diameter less than 10–40 μm, typically, among which mineralogical clays) that develop colloidal interactions. When the water content approaches the liquid limit LL, these soils typically turn into muddy slurries, although large, noncolloidal debris can also be present.

Rheological measurements on various types of colloidal suspensions and pastes show that these materials generally obey, in steady state, a viscoplastic-type constitutive law (e.g., Coussot 2005). They behave as soft solids when the applied stress lies below a critical stress threshold (or yield stress) τ_c and flow as viscous fluids above this threshold. Although only few studies attempted to directly characterize the rheological behavior of clay soils and muds originating from landslides (e.g., Coussot et al. 1998; Picarelli et al. 2004; Malet et al. 2003, 2005), existing ones show that these natural materials can also be described by viscoplastic laws for sufficiently high water contents. The evolution of critical shear stress τ_c with water content and particle properties (e.g., size distribution, mineralogy, etc.), however, remains poorly understood. For fine-grained sediments, a few authors (Locat and Demers 1988; Locat 1997; Jeong et al. 2010) proposed empirical relations between τ_c and the geotechnical liquidity index LI = (w–PL)/PI. Water salinity and ionic content were also shown to have an influence on the critical stress (Locat 1997; Jeong et al. 2010, 2012; Maio and Scaringi 2016). For debris flows, the critical shear

stress τ_c was shown to be highly sensitive to the type of clays (in particular, swelling clays) present in the material (Bardou et al. 2007). More fundamental studies indicated that, in general, the influence of fine and coarse particle fractions should be distinguished (Coussot and Piau 1994; Ancey and Jorrot 2001). The critical stress τ_c is reported to increase exponentially with the concentration in fine colloidal particles (Coussot and Piau 1994; Coussot 1995; Ancey and Jorrot 2001). An increase in τ_c with the addition of coarse, noncolloidal, particles is also observed, but at a smaller rate (Ancey and Jorrot 2001; Ovarlez et al. 2015; Dagois-Bohy et al. 2015). A primary objective of this study was then to investigate how the critical shear stress τ_c of clay landslides vary, and how these variations can be rationalized in terms of geotechnical parameters of the material.

In addition to viscoplasticity, colloidal materials are also frequently characterized by thixotropy, i.e., time/history dependence of the critical shear stress τ_c, and by the existence of a critical shear rate $\dot{\gamma}_c$ below which the material cannot flow (Coussot et al. 2002a, b; Coussot 2005). This critical shear rate is associated to an abrupt viscosity drop (or bifurcation) at the solid-fluid transition, potentially leading to catastrophic fluidization phenomena (Coussot 2005; Huynh et al. 2005, Khaldoun et al. 2009). Recently, rheometrical tests performed on natural clay samples originating from the Trièves area (a French Alps region affected by numerous landslides) also revealed a thixotropic behavior with a highly pronounced viscosity bifurcation (Mainsant et al. 2012b, 2015). In addition, this bifurcation was accompanied by a severe drop in elastic shear modulus G, suggesting that this parameter (or, alternatively, the shear wave velocity $Vs = (G/\rho)^{1/2}$, where ρ is the bulk density of the soil), which characterizes the rigidity of the soil, could actually constitute a proxy for the solid-fluid transition. A second objective of this study was therefore to investigate whether these complex rheological trends are also observed with other clay landslides and, more generally, to assess whether soils coming from clayey landslides exhibit similar rheological properties at the solid-fluid transition.

This paper thus reports on a detailed geotechnical and rheometrical characterization of soil samples from six different clayey landslides across Europe. These landslides were chosen because they gave rise to mud or debris flows in the past and appear prone to slide-to-flow transitions. The main morphological features of the landslides and the experimental methods used to characterize the material samples are first briefly described. We then summarize the geotechnical and rheological properties of the samples, with a particular focus on critical shear stress τ_c, critical shear rate $\dot{\gamma}_c$, and shear modulus G (as well as the corresponding shear wave velocity V_s). Finally, the existence of relations among these different properties is investigated, and the possible implications of our laboratory results at field scale are discussed.

Site description

Clayey soils were sampled at six landslide sites having experienced flow-like motions: Harmalière (HA), Super-Sauze (SU), and Char d'Osset (CO) in the French Alps, Hollin-Hill (HO-England), Montevecchio (MO-Northern Apennines, Italy), and Pont-Bourquin (PO-Switzerland). The location of the landslides and their geometry are shown in Fig. 1. Pictures of the landslides are shown in Fig. 2 and their main characteristics are given in Table 1. The landslides have developed in geological formations of various ages (from Lias to Quaternary) and exhibit a large variety in shape, surface area, and volume (from approximately 35×10^3 m^3 for PO to 25×10^6 m^3 for HA) (Table 1). Only one landslide affects the in situ geological bedrock itself (quaternary glaciolacustrine deposits at HA). In all other sites, the moving mass is made of weathered clay sliding on the parent rock. In terms of slope angles, the HA, HO, and MO landslides exhibit gentle slopes ranging from 9° to 12°. In contrast, the PO, SU, and CO landslides have a more abrupt morphology with slope angles between 25° and 33°. Three landslides are channelized (SU, CO, and MO), with a high length/width ratio ranging from 6 to 23 (Figs. 1 and 2). The Harmalière landslide is channelized in its lower part only and exhibits a length/width ratio of 1.8. In contrast, the HO landslide exhibits a length/width ratio lower than 1, while the PO landslide is elongated.

The maximum measured displacement rates range from 0.01 m year^{-1} at HO to more than 50 m year^{-1} at SU. According to Hungr et al. (2014), these landslides can therefore be described as very slow to moderately slow earthflows. The CO landslide is dormant at the present time. Information about recorded mud flow and debris flow events is also given in Table 1, including the flow volume, their velocity (when known), and their mobility coefficient (or Heim coefficient: ratio height/length, H/L). The CO and SU sites are characterized by clayey soils having a high content of rocks or debris, while the other four sites are characterized by clayey soils with low content of rocks or debris. Size distribution measurements made on the 6 sites show that the complete material passes through the 400 μm sieve, except for Pont-Bourquin and Super-Sauze soils. Although no size distribution measurements could be made on the soil of Char d'Osset, field observations indicate that the fraction of grains passing through the 400 μm should be less than 50%. To highlight the different grain-size compositions, we call "debris flows" (DF) the flow-like landslides originated in clayey soils enriched with debris (CO and PO SU sites) and "mud flows" those generated in clayey soils with low debris content (HA, MO, HO sites). The volume and velocity of these flow events can vary significantly among the sites. For example, at SU, several debris flows were reported with volumes of a few thousand m^3 and velocities as high as 4 m s^{-1}, while the MO landslide experienced mud flows of about 90×10^3 m^3 flowing at approximately 5 m day^{-1}. The *H/L* coefficient of these flow events, which varies inversely with the mobility, also exhibits a large range of values with low values of 0.16 and 0.17 for the HO, HA, and MO landslides (showing high mobility), and higher values of 0.3 and 0.45 (hence lower mobility) for SU and PO. More detailed geomorphological and geological information about the six landslides can be found in the supporting information of this paper.

Methods

Geotechnical and mineralogical characterization

The clay soils were collected at a depth of approximately 0.3 m on the six landslides. All samples were sieved and particles with a size smaller than 400 μm were retained. Resulting particle size distributions were measured using a laser analyzer (Malvern Mastersizer 2000, https://www.malvernpanalytical.com/en/support/product-support/mastersizer-range/mastersizer-2000).

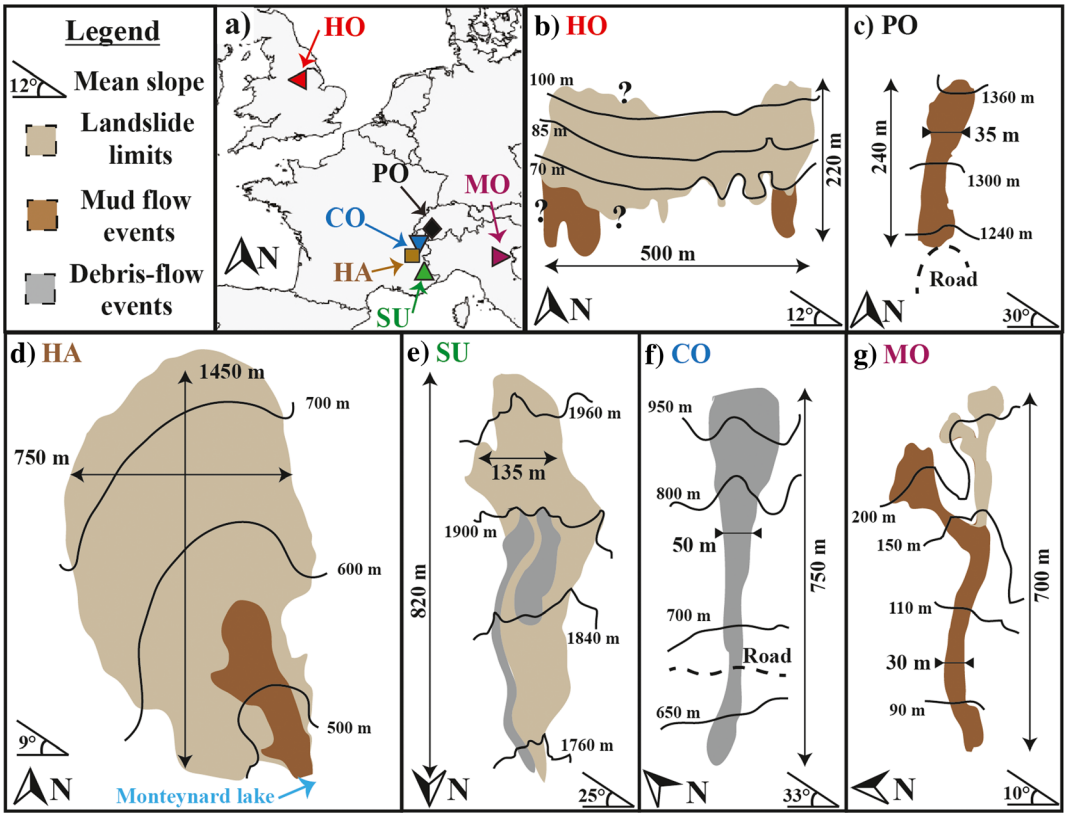

Fig. 1 Location (**a**) and simplified morphological maps of the six landslides: **b** HO: Hollin-Hill, **c** PO: Pont-Bourquin, **d** HA: Harmalière, **e** SU: Super-Sauze, **f** CO: Char d'Osset, and **g** MO: Montevecchio. The mud flow and debris flow events are differentiated by their brownish and gray color, respectively. As the CO landslide only evolves sporadically to a debris flow, the site is shown in gray with the limits of the last debris flow of 2011. The western part of the HO landslide is covered by trees, making it difficult to assess the exact limits of the earthflow

Identification of crystalline materials in the samples was performed through X-ray diffraction (XRD) using a Bruker D8 diffractometer. XRD patterns were recorded from randomly oriented powders. No attempt was made at quantifying amorphous materials that are possibly present in the samples.

The Atterberg limits of the 400-μm sieved samples were measured using the cup apparatus for the liquid limit (LL) and the rolling test method for the plastic limit (PL), applying European norm CEN/ISO/TS 17892-12. The gravimetric water content w (in %) was measured as M_w/M_s, where M_w is the mass of water in the sample and M_s is the mass of dried soil. The plasticity index PI = LL-PL and liquidity index LI = (w-PL)/PI were derived from these measurements. Methylene blue (MB) absorption tests were conducted to determine the specific surface area S_s of the clay particles (Santamarina et al. 2002) according to the European norm EN 933-9. The cation exchange capacity (CEC, expressed in milliequivalents (meq) per 100 g of dry solid) was measured through exchange with cobaltihexamine and dosing of its residual concentration in the equilibrium solution using a UV-visible spectrophotometer and cobaltihexamine ion absorption band at 472 nm.

Rheometrical characterization

Rheometrical tests were performed using a Bohlin-CVOR instrument with a 60 mm parallel-plate tools (see Fig. 3a). With this geometry, relatively thick samples can be tested (as required to consider the tested mixtures as continuum materials) while the shear stress and shear rate within the samples can still be determined accurately (Coussot 2005). The gap between the plates (sample thickness) was kept constant at 3600 μm for all tests. This value, approximately ten times larger than the maximum grain size in the samples, was found to be a good compromise to minimize end effects that develop with thicker samples. Two sets of tools, in PVC and stainless steel, respectively, both roughened to prevent wall slip, were used to check for repeatability of the results. The tests were carried out in an air-conditioned room, and the temperature of the samples was maintained constant at 21 °C during the experiments. Before each test, the samples were presheared at a shear rate of 50 s^{-1} for 20 s and then left at rest for 10 s to ensure a reproducible initial state. Samples at different water contents were prepared by mixing the dried soils with distilled water in a blender. It was only possible to test samples with a gravimetric water content w above the liquid limit LL. For $w < LL$, cracking and heterogeneous deformation were observed.

Two types of rheometrical protocols were applied to investigate the behavior of the clay soils in the vicinity of the solid-fluid transition. First, standard creep (SCr) tests, which consist in imposing a constant shear stress τ and monitoring the resulting shear rate, were used to determine the critical shear stress τ_c and critical shear rate γ_c of the samples. Four typical SCr tests obtained for PO soils at a water content w = 87.4% (LI = 3.66) are shown in Fig. 3b. At low imposed stress (τ = 30 Pa), the shear rate regularly decreases to reach values lower than 10^{-4} s^{-1} at the end of the test, which corresponds to a solid behavior. Conversely, at high stress

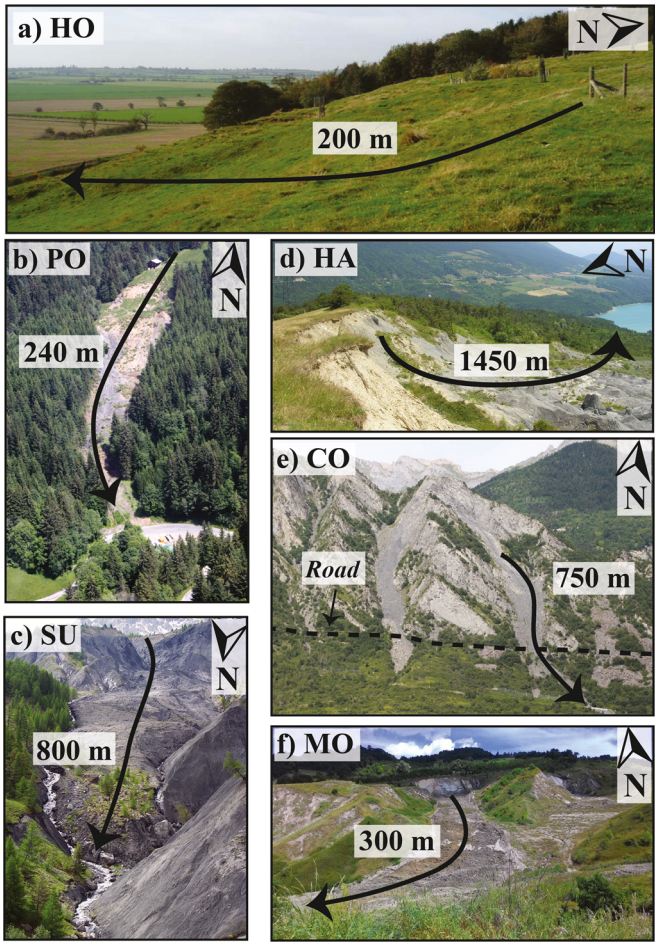

Fig. 2 Pictures of the six landslides. **a** Hollin-Hill (HO), **b** Pont-Bourquin (PO), **c** Super-Sauze (SU), **d** Harmalière (HA), **e** Char d'Osset (CO), and **f** Montevecchio (MO) landslides. The arrows show the movement direction and gives an order of magnitude of the distance

($\tau = 60$ Pa), the shear rate tends towards a constant value that increases with the imposed stress level, as for a viscous fluid. These observations are consistent with a viscoplastic behavior of the material. The critical shear stress, here $\tau_c \approx 53$ Pa, can be defined as the stress level for which the transition between these two regimes occurs. To obtain a good accuracy, multiple tests with stress increments of 1 to 5 Pa were performed in the vicinity of the solid-fluid transition. In some cases, however, it was difficult to determine whether the sample is effectively in solid or fluid regime within a range of a few Pa. In practice, the value of τ_c is thus taken as the average between the lowest stress value for which the sample is surely in fluid regime, and the highest stress value for which it is surely in solid regime. Depending on the suddenness of the transition and the repeatability of the results, which vary among the samples, the corresponding uncertainty on τ_c ranges between 5 and 15%. In the example of Fig. 3b, the solid-fluid transition is also characterized by a marked jump in shear rate, which discontinuously passes from zero in solid regime to a finite value when the stress is just above the critical stress. This behavior is characteristic of a viscosity bifurcation, with the existence of a critical shear rate $\dot{\gamma}_c$ below which no steady flow is possible. In practice, due to the abovementioned difficulties sometimes encountered in the determination of τ_c, we chose to define $\dot{\gamma}_c$ as the shear rate measured for $\tau = \tau_c + \Delta\tau$, where $\Delta\tau$ is a small stress increment above the transition taken equal to 5 Pa. This definition proved to be more robust, while still representative of the jump in shear rate observed at the transition. Hence, for PO sample at $w = 87.4\%$ (Fig. 3b), $\dot{\gamma}_c$ is taken at 2.5×10^{-2} s^{-1}, which corresponds to the asymptotic shear rate value reached in the test at 58 Pa.

Oscillatory creep (OCr) tests were used to capture the associated drop in elastic shear modulus at the solid-fluid transition. These tests consist of superimposing small stress oscillations to a constant average shear stress level τ (see Fig. 3a). The resulting strain is monitored and corrected for any linear trend associated to the average stress level. The complex viscoelastic modulus G^* is defined as the ratio between the stress and the detrended strain in the Fourier domain (Bird et al. 1987). The amplitude of the stress oscillations was chosen to be roughly 1/10 of the critical stress τ_c in order to remain in the linear regime. The frequency of the oscillations was fixed at 5 Hz in order to be in a regime where the storage modulus (i.e., the real part of G^*) is independent of the frequency and can be identified as the elastic shear modulus G of the clayey soil (Mainsant et al. 2012b). Four typical examples of OCr tests for PO soil at $w = 87.4\%$ are shown in Fig. 3c. A clear decrease in elastic shear modulus is observed when the soil fluidizes, with G dropping from values above 10,000 Pa when τ is just below τ_c (solid state), to values of about 1000–3000 Pa just above τ_c (fluid state). The shear elastic modulus then continues to rapidly decrease when the stress level is further increased, reaching very low values (100 Pa in the example shown) in the fully fluidized regime. We characterize the amplitude of the drop in G at the transition by the ratio of G_s/G_{tf}, where G_s and G_{tf} correspond to the values of G in the solid and fluid states, respectively. As for $\dot{\gamma}_c$, the value of G_{tf} is determined for $\tau = \tau_c + \Delta\tau$.

Geotechnical results

The grain size distributions of the six 400 µm sieved soils are shown in Fig. 4a. The values of D_{40} and D_2 (soil fractions below 40 and 2 µm, respectively), of the uniformity coefficient $C_u = d_{60}/d_{10}$, and of the curvature coefficient $C_c = (d_{30})^2/(d_{60}\, d_{10})$ are given in Table 2 (the diameter d_X correspond to the particle size for which X% of the particles are finer). All samples exhibit C_u values higher than 6 and C_c values around 1, indicating wide particle size distributions with unimodal shapes. CO and PO samples stand out as coarser than the others, as shown by their grain size distributions and their lower D_{40} values (48 and 60%, respectively).

As shown in Fig. 4b, the Atterberg limits show large variations among the different soils. Liquid limit *LL* ranges from very low (26.7%) for CO to high (73.3%) for HO. Plasticity index *PI* varies between 9.9% (CO) and 25.6% (HO and MO). According to the Unified Soil Classification System (USCS), four samples are described as low to medium plasticity clay soils (CO, SU, PO, and HA), while the other two are high plasticity clay soils (MO and HO). In addition, two of the soils are classified as organic (HO and PO). Blue methylene and *CEC* tests also highlight wide variations in clay properties among the samples. HO soil exhibits the highest values with a specific surface area S_s of 80.1 m^2 g^{-1} and a *CEC* of 28.6 meq 100 g^{-1}. In contrast, the CO sample is characterized by a low *CEC* (3.5 meq 100 g^{-1}) and extremely low specific surface area S_s (5.7 m^2 g^{-1}). In terms of mineralogical composition (Table 2),

Table 1 Geological, morphological, and kinematic characteristics of the Hollin-Hill (HO), Pont-Bourquin (PO), Harmalière (HA), Super-Sauze (SU), Char d'Osset (CO), and Montevecchio (MO) landslides. The characteristics of the earthflows, as well as those of the known mud flow (MF) and debris flow (DF) events, are given

Site		Hollin-Hill	Pont-Bourquin	Harmalière	Super-Sauze	Char d'Osset	Monte-vecchio
Geology and morphology	Geology	Lias, Whitby Mudstone	Aalenian black shales and flysch	Quaternary glaciolacustrine clays	Callovo-Oxfordian black marls	Eocene clayey flyschs	Holocene clayey and silty marl
	Sliding material	Weathered	Weathered	Parent	Weathered	Weathered	Weathered
	Length (m)	220	240	1450	820	400	700
	Width (m)	> 500	30–60	750	50–150	30–100	30–50
	Thickness (m)	2–5	5–10	10–50	8–30	5–10	8–10
	Surface (m^2)	100×10^3	8×10^3	10^6	170×10^3	24×10^3	28×10^3
	Volume (m^3)	$\approx 500 \times 10^3$	$\approx 35 \times 10^3$	$\approx 25 \times 10^6$	$\approx 750 \times 10^3$	$\approx 100 \times 10^3$	$\approx 350 \times 10^3$
	Slope (°)	12°	30°	9°	25°	33°	10°
	Maximum surface velocity (m $year^{-1}$)	0.01–2	3–6	0.1–7	50–100	0	0.1
	Channelized	No	Yes	Yes, in lower part	Yes	Yes	Yes
	% of fraction below 400 μm	100	65	100	50	?	100
Debris flows and mud flows	Flow type	MF	DF	MF	DF	DF	MF
	Volume	$100–200 \times 10^3$	$1–5 \times 10^3$	100×10^3	$2–8 \times 10^3$	10^3	90×10^3
	Velocity	Unknown	> 1 m s^{-1}	> 10 m h^{-1}	3–4 m s^{-1}	> 10 m h^{-1}	5 m day^{-1}
	Mobility H/L (Height/Length)	0.16	> 0.5	> 0.16	0.3	0.45	0.17

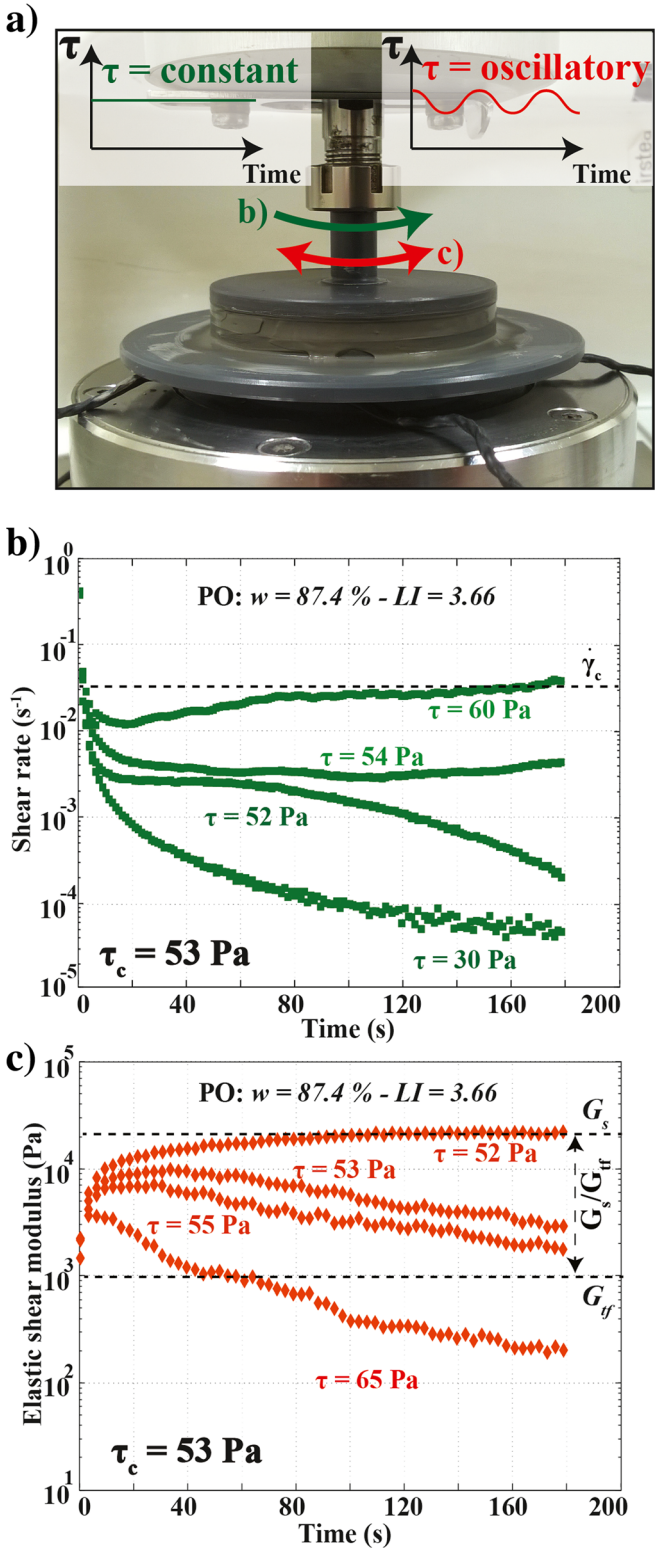

Fig. 3 Illustration of the rheometrical tests. **a** Picture of the Bohlin CVOR rheometer used to perform the standard creep tests SCr (constant stress with time—in green) and the oscillatory creep tests OCr (oscillatory stress with time—in red). **b** Four SCr tests performed at stress levels $\tau = 30$, 52, 54, and 60 Pa on PO (Pont-Bourquin) soil with a water content $w = 87.4\%$ (LI = 3.66). The increase in shear rate at the critical shear stress $\tau_c = 53$ Pa is indicative of the transition from solid to fluid state. **c** Four OCr tests performed below (52 and 53 Pa) and above (55 and 65 Pa) the critical shear stress τ_c for the same sample

most of the soils contain a significant amount of quartz and micas, from 19.6% (MO) to 54.8% (PO), with a fraction of clay minerals (all phyllosilicate but di-octahedral micas) varying between 4.3% (SU) and 45.6% (HO). Expendable 2:1 swelling clays, considered in this paper as smectites, have been detected in HO (33.8%), MO (15.3%), and HA (9.4%).

In summary, the soils collected at the six landslide sites exhibit strong differences in terms of geotechnical properties and mineralogical composition. HO and MO are the soils with the highest swelling potential, as shown by their large values of smectite content, *CEC*, and S_s. They also exhibit the highest values of *PI* and *LL*, indicating a high plastic potential. In contrast, the HA soil shows *PI* and *LL* values lower than those of MO and HO. This last sample contains nevertheless a significant amount of smectite (9.4%), resulting in relatively high *CEC* and S_s values. SU and PO are described by intermediate *CEC*, S_s, *PI*, and *LL* values and no smectite. Finally, CO has the lowest *CEC*, S_s, *PI*, and *LL* values.

As previously attempted by several authors (i.e., Farrar and Coleman 1967; Yukselen and Kaya 2006), we looked for potential relations among these different geotechnical parameters of the samples. In particular, Yukselen and Kaya (2006) proposed simple correlations between CEC, Atterberg limits, organic matter content, fine fraction, and specific surface area. As shown in Fig. 4c–e, the clay fraction D_2, the percentage of smectites, the Atterberg parameters *PL*, *LL*, and *PI*, and the specific surface area S_s all appear to be positively correlated to the *CEC*. The highest determination coefficients are obtained between the specific surface area and the CEC (0.95) and between the percentage of smectite and CEC (0.93). Conversely, the determination coefficient between D_2 and CEC is weak (0.33), and the determination coefficients between *PL*, *LL*, *PI*, and *CEC* are moderate (0.65, 0.86, and 0.86, respectively). It must be stressed that these results have been obtained for six samples only, and therefore cannot provide generic trends. They appear however in good agreement with the conclusions of Farrar and Coleman (1967) and Yukselen and Kaya (2006), which were based on more complete soil datasets. In particular, Yukselen and Kaya (2006) also reported a low determination coefficient between D_2 vs *CEC* ($R^2 = 0.37$), whereas they found better correlations between *CEC* and S_s ($R^2 = 0.82$), and between *CEC* and *LL* ($R^2 = 0.6$).

Rheometrical results

Standard creep (SCr) and oscillatory creep (OCr) tests were carried out on the six soils for 4 to 6 values of gravimetric water content *w* above the liquid limit *LL*. In Figs. 5 and 6, representative results are shown for two values of *w* that differ between the samples but always correspond to liquidity index *LI* approximately equal to 2 and 3, respectively.

In SCr tests at low water content ($LI \approx 2$, left column of Fig. 5), all samples exhibit a solid-fluid transition occurring at critical shear stress values ranging from 43 to 166 Pa. The CO sample displays the lowest critical stress, while the largest values correspond to MO and SU soils. The solid-fluid transition is marked by clear viscosity bifurcations for HO and MO samples, with critical shear rate values of the order of 10^{-1} s^{-1}. SU and CO soils display less pronounced viscosity bifurcations, with $\dot{\gamma}_c$ of the order of 10^{-2} s^{-1}, and the solid-fluid transition appears almost continuous for the PO and HA samples. If existent, $\dot{\gamma}_c$ values in these latter cases are very small, at most of the order of 10^{-2} s^{-1}. At a higher water content ($LI \approx 3$, right column of Fig. 5) solid-

fluid transitions are still observed for all samples, except for the CO soil for which the fluid regime seems reached even for the lowest shear stress values tested. Generally, the critical shear stress τ_c is observed to decrease when water content w increases. Conversely, the critical shear rate $\dot{\gamma}_c$ tends to increase with w. These trends are particularly marked for the HO sample, with a critical stress dropping from 127 to 40 Pa between $LI = 2$ and 3, respectively, and a concurrent increase in $\dot{\gamma}_c$ from 2×10^{-1} to more than 10 s^{-1}. PO and HA samples, for which a viscosity bifurcation was hardly observed at $LI = 2$, are characterized by values of $\dot{\gamma}_c = 10^{-2}$ s^{-1} and 4×10^{-2} s^{-1} at $LI = 3$, respectively.

OCr tests in Fig. 6 show the evolution of the elastic shear modulus G at the solid-fluid transition. Consistent with the results of (Mainsant et al. 2012b), the solid-fluid transition appears to be systematically accompanied, for all tested samples, by a decrease in G. We carefully ascertained that this decrease occurs for critical shear stress values which are identical, within experimental uncertainties, to the critical shear stress values determined in SCr tests. Values of G in the solid regime (G_s) are observed to decrease with the water content: they vary in the range 10^4–4×10^4 Pa for $LI = 2$, and in the range 5×10^3–2×10^4 for $LI = 3$. The drop in G at the transition, characterized by the ratio G_s/G_{tf}, appears to be variable among the samples. It is highly pronounced for HO and MO soils, in particular for $LI = 3$, where G drops by several orders of magnitude when increasing the stress level by only a few Pa beyond the critical stress. On the contrary, the drop in G at the transition is much smaller for HA, SU and PO soils for $LI = 2$, and the decrease in elastic modulus between the solid and fluid regimes appears more progressive in these cases. Generally, it is observed that the larger the amplitude of the viscosity bifurcation observed in SCr tests, the larger the associated drop in G at the solid-fluid transition. The elastic modulus then continues to decrease when the stress level is further increased beyond τ_c, and all samples are eventually characterized, in the "fully-fluidized" regime, by G values that are at least one order of magnitude smaller than G_s.

Discussion

The occurrence, in fixed-volume rheometrical tests, of a solid-fluid transition for a well-defined value of critical shear stress τ_c, is a hallmark of viscoplastic rheological behavior. Granular suspensions, on the contrary, tend to be characterized by an absence of yield stress in such a configuration (Boyer et al. 2011; Trulsson et al. 2015). Hence, all soil samples tested in this study effectively exhibit a viscoplastic behavior, except for CO soil at high water content for which no critical stress could be measured. This latter soil is also characterized by the lowest plasticity index PI, the lowest CEC and S_s values, and the lowest amount of fine particles. According to these characteristics, and although further tests would be required to confirm this conclusion, we may assume that CO soil actually presents a rheological behavior that is more of the frictional-type, particularly when the water content is high. This soil will not be taken into account in the upcoming analyses, in which only samples exhibiting a clear viscoplastic behavior will be considered.

Evolution of the critical shear stress

Our results for the five soils exhibiting a viscoplastic behavior show a clear increase in the critical shear stress τ_c when the water content w decreases (Fig. 7a), i.e., when the solid fraction Φ increases ($\Phi = 1/(1 + w.\rho_s)$ where ρ_s is the solid dry density, taken equal to 2.7 g cm^{-3}) since all samples are saturated. However, values of τ_c may vary by almost a factor of 2 among the different soils for a given solid fraction (Fig. 7a), and no generalized trend is apparent among the samples. This indicates that other parameters beyond the volume fraction also have an influence on the critical stress. In particular, it is known that fine (colloidal) and coarse (noncolloidal) particles contribute differently to the critical shear stress (Coussot and Piau 1994; Ancey and Jorrot 2001; Ovarlez et al. 2015), and that the critical shear stress is therefore also sensitive to the grain size distribution of the samples. In our study, large differences in D_{40} (see Table 2), and therefore in the relative proportions of fine and coarse particles, can be noted between the different clay soils. This is likely to partly explain the specific evolutions of τ_c as a function of the solid fraction (or water content) observed for each soil. We thus examined whether the variations of τ_c could be rationalized in terms of the geotechnical characteristics of the samples.

In an early study on sensitive clays, Locat and Demers (1988) proposed relations between the critical shear stress τ_c and the liquidity index LI. The parameter LI, in which the water content w is scaled by Atterberg's limits PL and LL, indirectly accounts for fine content and clay surface properties (through the existence of relations between D_2, PI, LL, CEC, and S_s, as shown in Fig. 4) (Locat and Demers 1988). These authors showed that τ_c values, obtained in their case through a fit of flow curves measured with a laboratory rheometer, could be bounded by the two following relations:

$$\tau_c = \left(\frac{12.05}{LI}\right)^{3.13} \quad (1)$$

for high pore salinity (30 g L^{-1}), and

$$\tau_c = \left(\frac{5.81}{LI}\right)^{4.55} \quad (2)$$

for low pore salinity (0 g L^{-1}).

Subsequently, Locat (1997) showed that these two bounding relations remain valid for different clay soils, mostly of glaciomarine origin, over a wide range of w and plasticity values. Values of τ_c versus LI corresponding to our samples are displayed in Fig. 7b, along with the two curves corresponding to Eqs. (1) and (2). It appears that all τ_c measurements are gathered around the high-salinity curve for low LI values, while some of the data tend to exceed this curve for high LI values. It must be stressed out that none of the soils studied here contain salts. The relative agreement between the high-salinity curve and our data may therefore be coincidental. In addition, Locat and Demers (1988) and Locat (1997) determined τ_c through a fit of the flow curves (using a Bingham model) while, in our study, τ_c values were obtained directly from creep tests (without any underlying model). τ_c values measured in these two different ways can show significant discrepancies (Bonn et al. 2015).

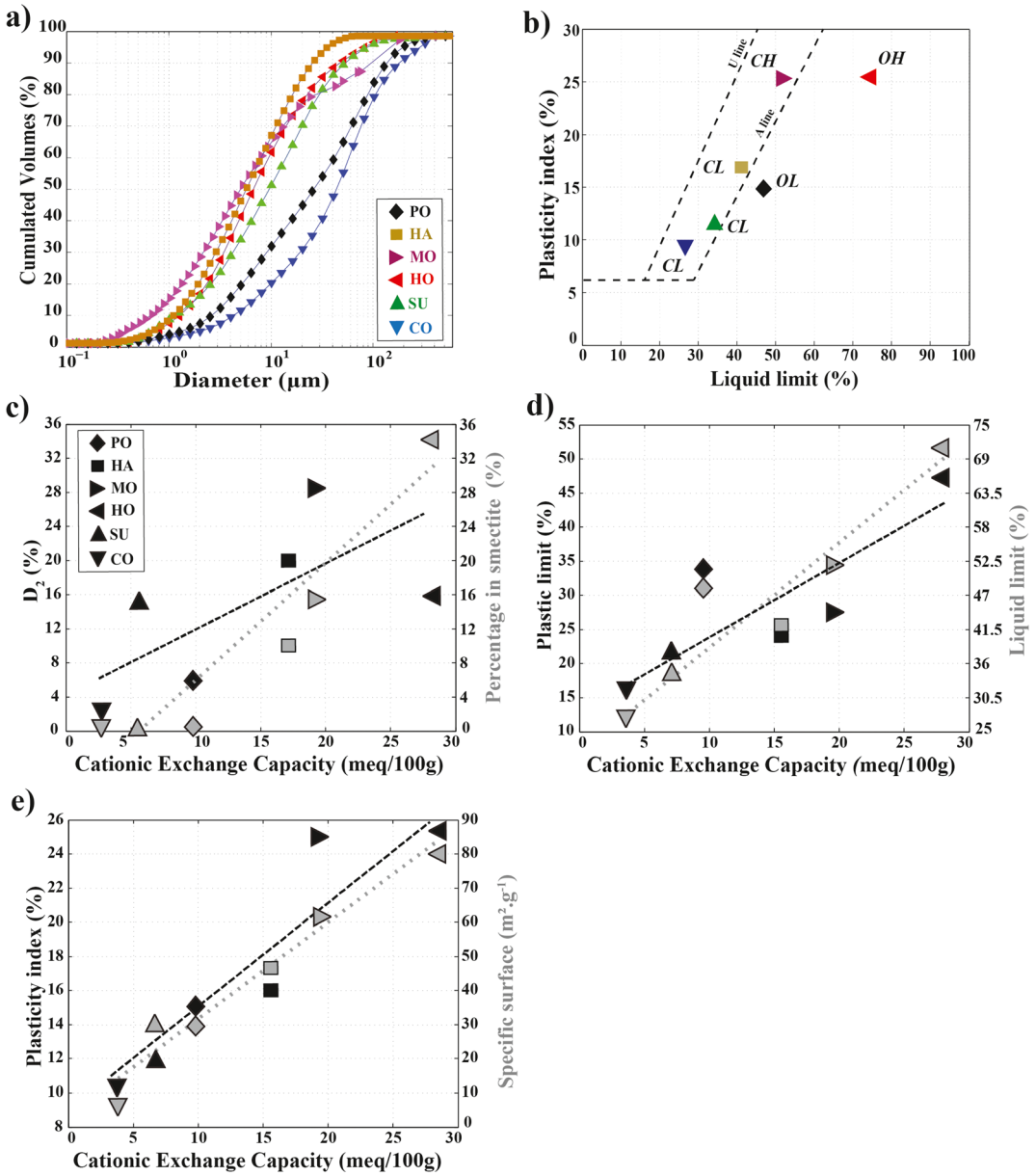

Fig. 4 **a** Grain size distribution of the six landslide samples sieved at 400 µm. **b** Casagrande's chart with the U and A lines (Mitchell 1993). According to the USCS classification, HA, SU, and CO samples are inorganic clayey soils of low to medium plasticity (CL). PO and HO are classified as organic clayey soils of low plasticity (OL) and high plasticity (OH), respectively. MO is defined as an inorganic clayey soil of high plasticity (CH). **c**–**e** Relationships between geotechnical, geochemical, and mineralogical parameters for the six clay samples. In all cases, measurement errors are smaller than marker sizes. **c** D_2 (soil fraction below 2 µm, in black dashed line) and percentage of smectite (in gray dotted line) versus CEC. Linear regressions on D_2 vs CEC data (black dashed line) and percentage of smectite vs CEC data (gray dotted line) yield determination coefficients $R^2 = 0.33$ and 0.93, respectively. **d** Atterberg limits PL and LL versus CEC. The determination coefficients obtained by linear regression are $R^2 = 0.65$ and $R^2 = 0.86$ for PL-CEC data (black dashed line) and LL-CEC data (gray dotted line), respectively. **e** Plasticity index and specific surface area versus CEC. Determination coefficients are 0.86 and 0.95 for PI-CEC and S_s-CEC data, respectively

Similarly, Locat and Demers (1988) used the cone penetration method for determining *LL*, while we applied the percussion technique, and it has been shown that liquid limits measured by the two methods are not necessarily identical (Sridharan and Prakash 2000). Given these differences, further quantitative comparisons between our results and those of Locat and Demers (1988) are not appropriate. A notable feature of Fig. 7b, however, is that the different soils follow specific trends according to *LI*. Hence HO and SU samples, which show similar τ_c values for $LI = 2.5$, strongly diverge when *LI* increases such that the value $\tau_c = 55$ Pa is reached for $LI = 3$ with the HO soil, and for $LI = 4.4$ with the SU soil. Correspondingly, the SU soil is characterized by a much lower liquid limit *LL* than the HO soil (33.3 and 73.3, respectively, see Table 1).

Table 2 Geotechnical and mineralogical characteristics of the six soil samples. D_{40} and D_2 represent the soil fraction below 40 and 2 μm, respectively. $C_u = d_{60}/d_{10}$, where d_{60} and d_{10} are the diameters for which 60 and 10% of the particles are finer. $C_c = (d_{30})^2/(d_{60}\, d_{10})$. USCS classification: CL stands for inorganic silty clays of low to medium plasticity; OL organic clays of low plasticity; CH inorganic clays of medium to high plasticity; OH organic clays of medium to high plasticity. The complete XRD results are presented in Table 3 of this paper

	Hollin-Hill	Pont-Bourquin	Harmalière	Super-Sauze	Char d'Osset	Monte-Vecchio
D_{40}–D_2 (%)	90–16	60–6	98–20	88–15	48–3	83–29
C_u	6.7	14.3	6.7	8.7	11	11.4
C_c	1.1	0.7	0.8	0.9	1.5	0.9
Liquid limit LL (%)	73.3 ± 0.8	47.7 ± 0.7	39.0 ± 0.2	33.3 ± 0.9	26.7 ± 0.4	51.7 ± 0.5
Plasticity index PI	25.6 ± 1	14.9 ± 0.9	16.9 ± 0.2	11.9 ± 0.8	9.9 ± 1	25.6 ± 0.8
USCS classification	OH	OL	CL	CL	CL	CH
Specific surface area S_s ($m^2\ g^{-1}$)	80.1 ± 4.2	29.2 ± 0.3	45.1 ± 0.3	29.6 ± 1	5.7 ± 0.5	61.6 ± 0.4
C.E.C (meq.100 g^{-1})	28.6	9.9	17.0	6.2	3.5	18.7
XRD (%)						
Quartz	21.8	16.5	18.9	23.9	20.9	15.5
Dioct. micas	20.1	54.8	28.9	37.3	33.4	19.6
Clay minerals	45.6	9.9	16.3	4.3	15.2	41
Expandable 2:1 clay	33.8	Ø	9.4	Ø	Ø	15.3

Detailed examination of Fig. 7b led us to change the scaling of w and plot τ_c directly versus the quantity w-LL. As shown in Fig. 7c, this representation leads to an interesting gathering of all the data on a common linear trend (in log-linear coordinates). The data can be fitted by the following exponential law with a determination coefficient $R^2 = 0.91$:

$$\tau_c = 246.7 \exp\left(-0.034(w-LL)\right) \quad (3)$$

with τ_c in Pa, w and LL in %. The quantity w-LL thus appears as a major control parameter for the critical shear stress values measured in this study. This parameter includes the effect of solid fraction Φ as well as, through the Atterberg liquid limit, the effects of fine content and clay properties. Nevertheless, the fact that such a simple measure of the deviation of w from LL is sufficient to account for critical shear stress values measured in a variety of different clay soils can seem surprising. It can be argued, however, that the existence of a relation between LL and the shear strength (measured here by the critical shear stress) of the soil is not entirely unexpected. In the percussion method used to determine LL (with Casagrande cup), the soil mass flows on both sides of the cup due to impacts on the base. According to Sridharan and Prakash (2000), this flow is viscous and controlled by the shear strength of the soil. Along the same line, Haigh (2012) recently found that LL is a function of the ratio between the undrained shear strength and the density of the material. These prior studies provide some support to our results, showing that the parameter w-LL may be used to predict the critical shear stress τ_c, disregarding the nature of the clay soil.

Evolution of viscosity and elastic bifurcations

The critical shear rate $\dot{\gamma}_c$ characterizing the amplitude of the viscosity bifurcation at solid-fluid transition for the different soils tested is plotted against the deviation w-LL in Fig. 7d. As already noted, for each soil, $\dot{\gamma}_c$ shows a clear increase with the water content w. Furthermore, it is observed that the data here also roughly collapse on a single relation of w-LL. Fitting an exponential law of the form $a.\exp(b.(w\text{-}LL))$ yields the following coefficients: $a = 6.9 \times 10^{-3}\ s^{-1}$; $b = -0.0712$, and a determination coefficient $R^2 = 0.56$. This latter value shows that the dispersion around this mean trend is significantly larger than in the case of the critical shear stress τ_c. For similar values of w-LL, differences as large as one order of magnitude are observed between the critical shear rates $\dot{\gamma}_c$ measured for the different samples (Fig. 7d). As already pointed out, for some of the samples, the existence of a viscosity bifurcation can even be questioned (typically, when the reported values of $\dot{\gamma}_c$ are less than$10^{-2}\ s^{-1}$). Hence, even if the deviation w-LL appears again to be an important control parameter, this parameter is not sufficient to fully account for the existence and magnitude of the viscosity bifurcations in the different studied clay soils. The presence of smectite, in particular, seems to also play a significant role, as the two soils exhibiting the highest values of $\dot{\gamma}_c$ (HO and MO) are also those with the highest proportion of swelling clays (see Table 1). It can also be noted that HO soil, for which the fraction of smectite is the largest (33.8%), presents a peculiar behavior at high water content. Above w-$LL = 50\%$, the magnitude of the viscosity bifurcation abruptly increases with a value of $\dot{\gamma}_c$ jumping from 0.2 to 20 s^{-1} (note that the values

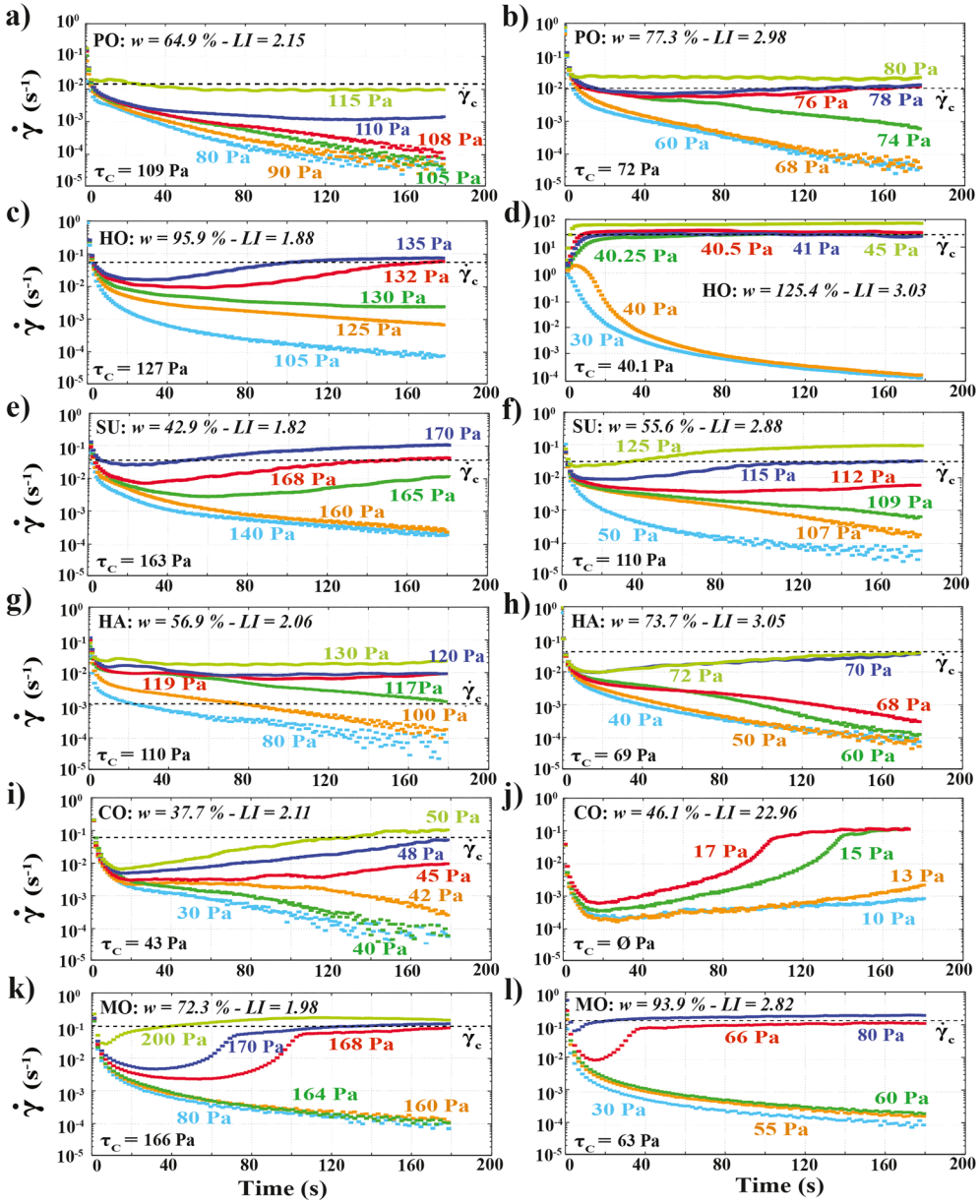

Fig. 5 Shear rate $\dot{\gamma}_c$ vs time curves measured during Standard Creep tests (SCr) conducted on Pont-Bourquin (PO, **a**, **b**), Hollin-Hill (HO, **c**, **d**), Super-Sauze (SU, **e**, **f**), Harmalière (HA, **g**, **h**), Char d'Osset (CO, **i**, **j**), and Montevecchio (MO, **k**, **l**) samples for two values of liquidity index approximately equal to 2 (left column) and 3 (right column). Corresponding water contents w are indicated in legend. The critical shear stress τ_c and critical shear rate $\dot{\gamma}_c$ inferred from the tests (see "Methods" section) are indicated for each sample

of $\dot{\gamma}_c$ measured for HO samples above the jump were not taken into account in the exponential trend presented above).

Similarly, the ratio G_s/G_{tf}, which characterizes the amplitude of the drop in elastic shear modulus at the solid-fluid transition, is shown as a function of *w-LL* in Fig. 7e. In Fig. 7f, we also show the evolution of the solid state elastic shear modulus G_s versus *w-LL*. Since the elastic modulus of the samples systematically reaches very low values (compared to G_s) in the fluid regime, the value of G_s can be considered as representative of the total drop in elastic shear modulus between the solid and fluid regimes. For all soil samples, the ratio G_s/G_{tf} increases, while on the contrary the value of G_s decreases with the water content. Here again, simple relations with the deviation *w-LL* appear to reasonably capture the main trends of these parameters. Fitting exponential laws of the form $a.\exp(b.(w\text{-}LL))$ yields the following coefficients: $a = 1.85$, $b = 0.074$ and a determination coefficient $R^2 = 0.64$ for the ratio G_s/G_{tf}, and $a = 4.5 \times 10^4$ Pa, $b = -0.036$ and $R^2 = 0.72$ for G_s. We also note that MO and HO samples, which are characterized by the highest smectite content, stand out by showing the lowest G_s values and, for HO, a jump in G_s/G_{tf} for *w-LL* > 50%.

Finally, it can be concluded that the first-order trends shown by the different mechanical properties of the clay soils

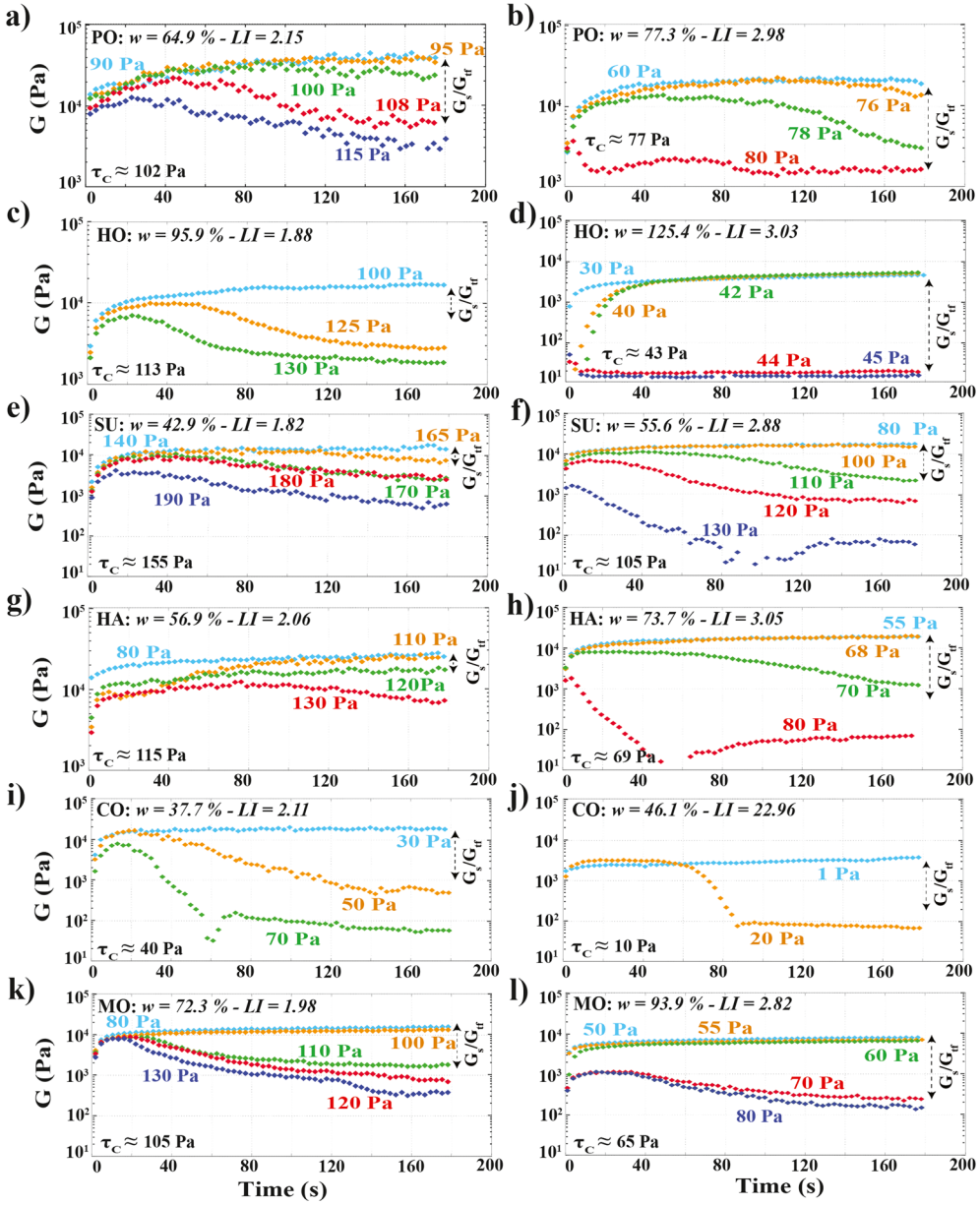

Fig. 6 Elastic shear modulus G vs time measured during oscillatory creep tests (OCr) on Pont-Bourquin (PO, **a**, **b**), Hollin-Hill (HO, **c**, **d**), Super-Sauze (SU, **e**, **f**), Harmalière (HA, **g**, **h**), Char d'Osset (CO, **i**, **j**), and Montevecchio (MO, **k**, **l**) samples for two values of liquidity index approximately equal to 2 (left column) and 3 (right column). The values of the critical shear stress τ_c obtained in SCr tests are recalled. The ratio between G_s and G_{tf} (see "Methods" section) is used to quantify the drop in G at the solid-fluid transition

at the solid-fluid transition (τ_c, $\dot{\gamma}_c$, G_s/G_{tf}, G_s) are all explained by exponential relations with the deviation *w-LL*. However, claiming that this parameter completely controls the rheological behavior of the studied soils would be abusive. Even if the liquid limit already partly accounts for the physicochemical properties of the materials, other parameters, and in particular the presence of swelling clay, also seem to have a significant influence on the viscosity and elastic bifurcations observed at the solid-fluid transition. To go further, it could be relevant to investigate second-order dependencies between the coefficients a and b characterizing the evolutions of $\dot{\gamma}_c$, G_s/G_{tf}, and G_s versus *w-LL* for each soil sample, and geotechnical properties such as *PI*, *CEC*, or smectite content. However, with the limited available data, no consistent relations could be found at this stage.

Extrapolation to field scale

To finish, we discuss the potential implications of our results for the prediction and understanding of slide-to-flow transition in clay landslides. A first striking feature is the existence of a marked viscosity bifurcation for some of the tested soils. As shown by Coussot (2005), we can expect materials exhibiting such characteristic to be particularly prone to catastrophic fluidization events, and to give rise to high-velocity mud or debris flows. On the

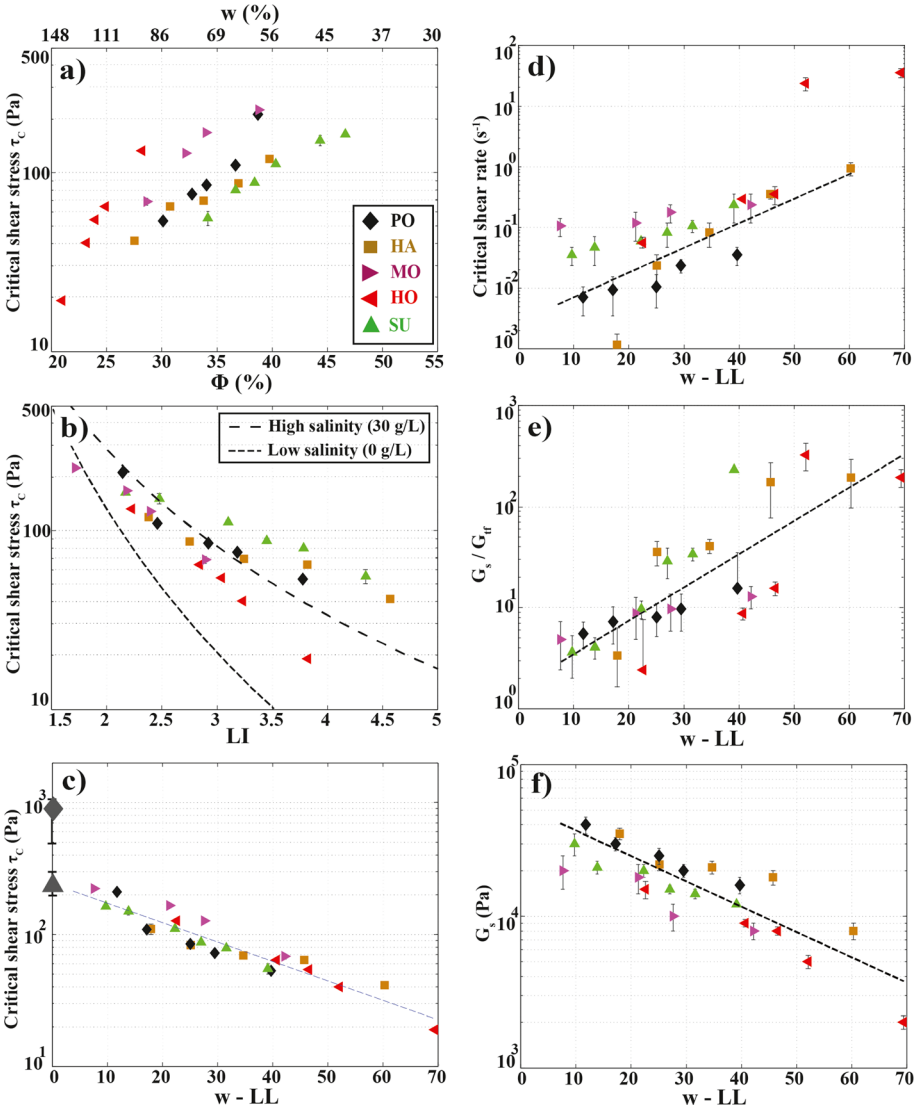

Fig. 7 **a**–**c** Variation of the critical shear stress τ_c measured during rheometric creep tests with **a** solid fraction Φ and gravimetric water content w, **b** liquidity index LI, and **c** the deviation of w from the Atterberg liquid limit, w-LL. In **b**, the power laws describing the evolution of τ_c with LI for high and low salinity (Locat 1997) are plotted. In **c**, the exponential law $\tau_c = 246.7 \exp(-0.034(w\text{-}LL))$ fits the data with a determination coefficient of 0.91. Gray markers in **c** correspond to yield stress values back-calculated from real debris flow events of PO and SU sites (see the "Extrapolation to field scale" section). **d**–**f** Variation of critical shear rate $\dot{\gamma}_c$, ratio of elastic shear modulus between solid and fluid regimes G_s/G_{tf}, and elastic shear modulus in solid regime G_s. with the deviation w-LL. Error bars are systematically plotted (when not visible, they are smaller than marker size). In **c**–**f**, dashed curves correspond to exponential fits of the data (see text)

contrary, soils without this property, or characterized by low values of $\dot{\gamma}_c$, are expected to transit more progressively from solid to fluid regimes, and thus to produce less catastrophic flow events. In this respect, the three landslides showing the highest values of $\dot{\gamma}_c$ in the experiments, at low and high water contents—namely HO, HA, and MO (Fig. 7d)—are also those for which the highest mobility flows have been observed (Table 1).

Also of particular interest is the excellent correlation observed between τ_c and w-LL (Eq. (3)) for the different tested soils. This result suggests that the critical shear stress of a landslide, i.e., the stress level at which solid-fluid transition occurs, might be evaluated and monitored directly from measurements of the water content w, provided the liquid limit LL is known. Following Hungr et al. (2014), who indicate that debris flows are likely to be triggered when materials are close to their liquid limit, our results could even imply that a unique critical stress value, on the order of 200–300 Pa (extrapolation of relation (3) to w-$LL = 0$, see Fig. 7c), could be used to predict the occurrence of such flow events. Care should nevertheless be taken concerning the representativeness of the critical stress values measured in our rheometrical tests, since these tests were not performed on the in situ soils, but on samples sieved at 400 µm. In fact, clay soils collected at MO, HA, and HO sites contain essentially no particles larger than 400 µm (see the "Site description" section). In these cases, the tested samples can thus effectively be considered as

representative of the complete materials. On the contrary, CH, SU, and PO landslides contain significant amounts of particles larger than 400 μm. According to existing studies on model materials (Ancey and Jorrot 2001, Ovarlez et al. 2015, Dagois-Bohy et al. 2015), we can expect the value of τ_c to increase with the addition of coarse grains. Yet, interestingly, Malet et al. (2004) back-analyzed the runout and thickness of past debris flow deposits at SU site using the flow code Bing (Imran et al. 2001) and reported a critical stress value of $\tau_c = 250 \pm 50$ Pa that is well within the range arising from our experimental results. We performed a similar back-analysis on a debris flow event that took place at PO site (see Appendix 2). In this case, the analysis yields a critical stress of $\tau_c = 900 \pm 400$ Pa, larger than our experimentally derived values but still within the same order of magnitude. These two back-calculated critical stress values have been represented in Fig. 7c at $w\text{-}LL = 0$. Although additional field cases would be needed to strengthen these results, the good agreement between the back-analyzed and laboratory-derived values tends to indicate that relation (3) could effectively be used to obtain at least first estimates of the critical stress of clay landslides at field scale, and this even when a coarse fraction > 400 μm is present in the material.

Finally, we turn to the measurements of elastic shear modulus G, and the systematic drop in G of at least one order of magnitude observed in all tested soils at the solid-fluid transition. This systematic drop, followed by a further decrease in G as the material fully fluidizes, is consistent with the decrease in seismic shear velocity V_s reported before the occurrence of flow events both in laboratory flume experiments (Mainsant et al. 2015) and in the field (Mainsant et al. 2012a). This indicates that a loss of rigidity at the solid-fluid transition can be considered as a generic feature of clay soils, and confirms that V_s variations constitute a good indicator for monitoring clay landslides. It shall be emphasized, however, that the values of G inferred from our OCr tests appear relatively low compared to typical field values. When converted into shear wave velocities through the simple relation $V_s = (G/\rho)^{1/2}$, our laboratory measurements correspond to V_s values ranging between 3 and 5 m s^{-1} in solid regime, and less than 1 m s^{-1} in fluid regime. As a comparison, typical values of V_s inferred from seismic noise measurements at the base of the PO landslide varied between 400 and 200 m s^{-1} typically, during the preparation of a flow event (Mainsant et al. 2012a). We interpret this quantitative discrepancy as resulting from the strong sensitivity of V_s, and thus of G, to the water content when the sample is below its liquid limit LL. Experiments performed by Mainsant et al. (2012b) on HA soil showed values of V_s as low as 10 m s^{-1} for samples at the liquid limit, consistent with our measurements, but values of V_s of more than 100 m s^{-1} for $w\text{-}LL = -10\%$. A strong decrease in G and V_s with porosity, resulting from clay deconsolidation, was also reported by Renalier et al. (2010) both from laboratory tests and field data. To complement our results, measurements of G at the solid-fluid transition for samples presenting water contents more representative of those typically found in the field, i.e., below LL, would thus be useful. Designing well-controlled experimental tests to monitor solid-fluid transition in such strongly plastic samples represents an interesting perspective for future work.

Conclusion

The solid-fluid transition in clay soil samples collected from six landslides producing flow-like events was studied in laboratory rheometrical tests. Creep and oscillation tests were performed to measure the critical shear stress τ_c, the critical shear rate $\dot{\gamma}_c$, and the elastic shear modulus G at the solid-fluid transition, as a function of the water content w. All soils, except for Char d'Osset landslide, exhibit a viscoplastic rheological behavior. The critical shear stress triggering solid-fluid transition varies among the samples and decreases with the water content. The particular behavior of Char d'Osset clay soil has been linked to its low specific surface and cation exchange capacity. The five other clay soils are also characterized by bifurcations in viscosity and marked losses of rigidity at the solid-fluid transition. The existence and amplitude of the viscosity bifurcation, as well as the amplitude of the concurrent drop in elastic shear modulus, appear to be influenced by the water content as well as by the presence of swelling clays in the samples.

An important result of our study is that all the viscoplastic soils, which come from landslides characterized by very different geomorphological features, obey a common exponential law relating τ_c and the deviation $w\text{-}LL$. This relation is further strengthened by the back-analyses of real flow events at PO and SU sites, which lead to critical stress values that are consistent with the extrapolation of the laboratory-derived exponential law for $w = LL$. Moreover, the consistency of the rheometric results between sieved soil samples (Pont-Bourquin, Super-Sauze) and the complete material (Montevecchio, Harmalière, and Hollin-Hill) also strengthen the $w\text{-}LL$ relationship. Similar simple exponential laws with $w\text{-}LL$ were also proposed for the critical shear rate and the drop in shear modulus, albeit with lower correlation coefficients. These results reveal that the deviation $w\text{-}LL$ could be a key parameter controlling the mechanical behavior of these clay soils at the solid-fluid transition. This parameter captures the first-order effects of both water content and solid fraction properties (grain size distribution, physicochemical characteristics, etc.). Our study can be regarded as a first attempt at linking the rheological behavior of clay landslides with simple geotechnical characterizations. It opens up promising prospects for landslide monitoring and suggests that w measurements could be used to assess the conditions for which a clay soil of known liquid limit LL can fluidize. Alternatively, these results highlight the potential value of geophysical monitoring (electrical resistivity and shear wave velocity) on landslides to gain insight in the rheological change in clay soils during slide-to-flow transition.

Acknowledgements

The authors thank Frédéric Ousset and Hervé Bellot from IRSTEA (rheometrical tests) and Martine Lanson and Nathaniel Findling from ISTerre (geochemical and mineralogical analyses) for their assistance. The authors acknowledge financial support from the French VOR federative structure, the ARC project from the Rhônes-Alpes region (France), and the CNRS through the INSU-TS-aléas program.

Appendix 1

Table 3 Mineralogical content of the soil samples

XRD (quoted as %)	Hollin-Hill	Pont-Bourquin	Harmalière	Super-Sauze	Char d'Osset	Montevecchio
Chlorite		7.4	6.9	4.3	15.2	
Kaolinite	11.8	2.5				25.7
Smectite	33.8		9.4			15.3
Di-octahedral micas	20.1	54.8	28.9	37.3	33.4	19.6
Pyrophyllite		5.3				
Quartz	21.8	16.5	18.9	23.9	20.9	15.5
Albite	3.1		4.8	7.3	12.5	4.5
K-spars	2.4		3.3			
Calcite		5.0	22.5	20.8	15.1	16.0
Aragonite					1.2	
Ankerite		6.5	1.8	5.6	0.8	3.4
Pyrite			0.2			
Magnetite						0.2
Goethite	4.8					
Lepidocrocite	0.8					
Anatase	0.7		2.0			
Rutile		2.2		0.7	1.0	
Jarosite	0.7					
Hornblende			1.3			
Total	100	100	100	100	100	100.2

Appendix 2. Back-analysis of Pont-Bourquin debris flow event

The Bing software (Imran et al. 2001) solves a 1D shallow-flow model relying on a viscoplastic rheology (Bingham or Herschel Bulkley) to simulate the propagation of debris flows. It has been initially developed for submarine debris flows, but can be adapted to subaerial flows by using an ambient fluid density equivalent to the air (1 kg m^{-3}). The computation of the flow starts from a semi-parabolic mass defined by a length and a thickness. The flow then propagates on an altimetric profile which is provided by the user.

Similar to Malet et al. (2004), we used this software to carry out a back-analysis of a debris flow event that occurred on the PO landslide in summer 2007 and was documented by Jaboyedoff et al. (2009). After heavy rainfalls, a flowing volume of about 11,000 m^3 cut the road at the toe of the landslide. A detailed geomorphological analysis provided the necessary information regarding the localization and size of the initial unstable mass. Accordingly, a maximum thickness of 3 m and a length of 100 m were used as initial conditions in Bing. Field observations after the event indicated a length of propagation of 130 to 160 m, and a front thickness of approximately 2 m on the road. In agreement with recommendations of Imran et al. (2001), numerical parameters were taken as follows: artificial viscosity = 10^{-4}; number of nodes in domain = 21; time step = 10^{-5} min. A Herschel-Bulkley viscoplastic law with an exponent $n = 0.25$ was used. In agreement with the common practice for muddy debris flows (Coussot et al. 1998; Rickenmann et al. 2006), the ratio τ_c/K between the critical stress τ_c and consistency K the material was considered constant, with values in the range 3–5 s^{-n}. Figure 8 shows the evolution of flow runout as a function of the considered critical shear stress and ratio τ_c/K. All the simulated-flows shown in Fig. 8 present front thicknesses between 1 and 2 m, in agreement with field values. It is observed that the simulated runout significantly decreases with the ratio τ_c/K. Depending on the value of this ratio, values of critical shear stress τ_c lying between 550 and 1300 Pa are necessary to reproduce the runout of the 2007 event.

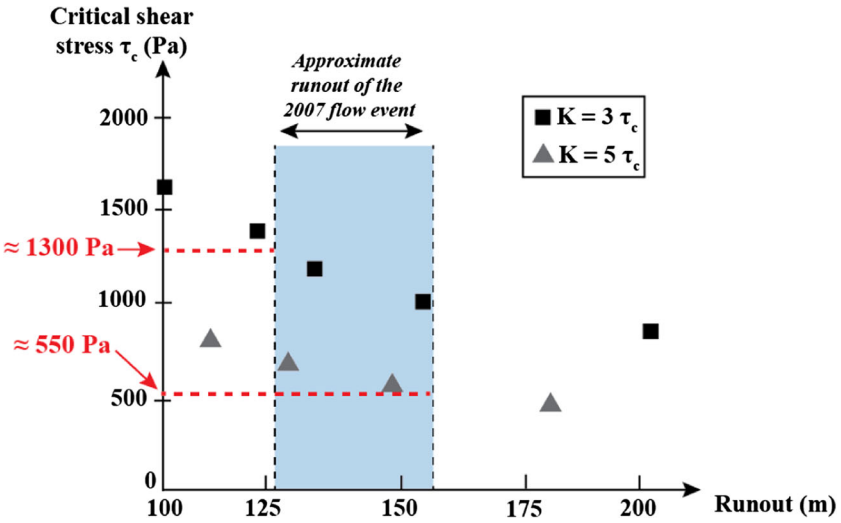

Fig. 8 Back-analysis of the 2007 flow event at Pont-Bourquin (PO) landslide with Bing software using a Herschel Bulkley viscoplastic law

References

Ancey C (2007) Plasticity and geophysical flows: a review. J Non-Newtonian Fluid Mech 142(13):4–35

Ancey C, Jorrot H (2001) Yield stress for particle suspensions within a clay dispersion. J Rheol 45(2):297–319

Bardou E, Bowen P, Boivin P, Banfill P (2007) Impact of small amounts of swelling clays on the physical properties of debris-flow-like granular materials. Implications for the study of alpine debris flow. Earth Surf Process Landf 32(5):698–710

Bièvre G, Jongmans D, Winiarski T, Zumbo V (2011) Application of geophysical measurements for assessing the role of fissures in water infiltration within a clay landslide (Trièves area, French Alps). Hydrol Process 26(14):2128–2142

Bird RB, Armstrong RC, Hassager O (1987) Dynamics of polymeric liquids, vol 1. John Wiley and Sons, New York

Bonn D, Paredes J, Denn MM, Berthier L, Divoux T, Manneville S (2015) Yield stress materials in soft condensed matter. Rev Mod Phys

Boyer F, Guazzelli E, Pouliquen O (2011) Unifying suspension and granular rheology. Phys Rev Lett 107:188301

Chambers JE, Wilkinson PB, Kuras O, Ford JR, Gunn DA, Meldrum PI, Pennington CVL, Weller AL, Hobbs PRN, Ogilvy RD (2011) Three-dimensional geophysical anatomy of an active landslide in Lias Group mudrocks, Cleveland Basin, UK. Geomorphology 125(4):472–484

Coussot P (1995) Structural similarity and transition from Newtonian to non-Newtonian behavior for clay-water suspensions. Phys Rev Lett 74:3971–3974

Coussot P (2005) Rheometry of pastes, suspensions, and granular materials, Wiley Online Library

Coussot P, Ancey C (1999) Rheophysical classification of concentrated suspensions and granular pastes. Phys Rev E 59:4445–4457

Coussot P, Piau JM (1994) On the behavior of fine mud suspensions. Rheol Acta 33(3):175–184

Coussot P, Laigle D, Arattano M, Deganutti A, Marchi L (1998) Direct determination of rheological characteristics of debris flow. J Hydraul Eng 124(8):865–868

Coussot P, Nguyen QD, Huynh HT, Bonn D (2002a) Viscosity bifurcation in thixotropic, yielding fluids. J Rheol 46(3):573–589

Coussot, P.; Nguyen, Q. D.; Huynh, H. T. & Bonn, D. (2002b) Avalanche behavior in yield stress fluids. Phys Rev Lett 88 - Number 17–5501, 4p

Dagois-Bohy S, Hormozi S, Guazzelli E, Pouliquen O (2015) Rheology of dense suspensions of non-colloidal spheres in yield-stress fluids. J Fluid Mech 776

Farrar DM, Coleman JD (1967) The correlation of surface area with other properties of nineteen British clay soil. J Soil Sci 18(1):118–124

Haigh SK (2012) Mechanics of the Casagrande liquid limit test. Can Geotech J 49(9):1015–1023

Hungr O, Leroueil S, Picarelli L (2014) The Varnes classification of landslide types, an update. Landslides 11(2):167–194

Huynh HT, Roussel N, Coussot P (2005) Aging and free surface flow of a thixotropic fluid. Phys Fluids 17:033101

Imran J, Harff P, Parker G (2001) A numerical model of submarine debris flow with graphical user interface. Comput Geosci 27(6):717–729

Iverson RM (1997) The physics of debris flows. Rev Geophys 35(3):245–296

Iverson RM (2005) Regulation of landslide motion by dilatancy and pore pressure feedback. J Geophys Res: Earth Surf 110(F2)

Iverson RM, George DL (2016) Modelling landslide liquefaction, mobility bifurcation and the dynamics of the 2014 Oso disaster. Géotechnique 66(3):175–187

Jaboyedoff, M.; Pedrazzini, A.; Loye, A.; Oppikofer, T.; i Pons, M. G. & Locat, J.Malet, J.-P.; Remaitre, A. & Bogaard, T., ed. (2009), Earth flow in a complex geological environment: the example of Pont Bourquin, Les Diablerets (Western Switzerland), Landslide Processes, From Geomorphologic Mapping to Dynamic Modelling

Jeong SW, Locat J, Leroueil S, Malet J-P (2010) Rheological properties of fine-grained sediment: the roles of texture and mineralogy. Can Geotech J 47(10):1085–1100

Jeong SW, Locat J, Leroueil S, Malet J-P (2012) The effects of salinity and shear history on the rheological characteristics of illite rich clays. Clay Clay Miner 60:108–120

Khaldoun A, Moller P, Fall A, Wegdam G, De Leeuw B, Méheust Y, Fossum J, Bonn D (2009) Quick clay and landslides of clayey soils. Phys Rev Lett 103:188301

Locat J (1997) Normalized rheological behavior of fine muds and their flow properties in a pseudoplastic regime', Debris-flow hazards mitigation: mechanics prediction and assessment, Water Ressources Engineering Division. Am Soc Civil Eng 260–269

Locat J, Demers D (1988) Viscosity, yield stress, remolded strength, and liquidity index relationships for sensitive clays. Can Geotech J 25(4):799–806

Mackey BH, Roering JJ, McKean JA (2009) Long-term kinematics and sediment flux of an active earthflow, Eel River, California. Geology 37(9):803–806

Mainsant G, Jongmans D, Chambon G, Larose E, Baillet L (2012a) Shear-wave velocity as an indicator for rheological changes in clay materials: lessons from laboratory experiments. Geophys Res Lett 39(19), 5p

Mainsant G, Larose E, Brönnimann C, Jongmans D, Michoud C, Jaboyedoff M (2012b) Ambient seismic noise monitoring of a clay landslide: toward failure prediction. J Geophys Res: Earth Surf 117(F1)

Mainsant G, Chambon G, Jongmans D, Larose E, Baillet L (2015) Shear-wave-velocity drop prior to clayey mass movement in laboratory flume experiments. Eng Geol 192:26–32

Maio C, Scaringi G (2016) Shear displacements induced by decrease in pore solution concentration on a pre-existing slip surface. Eng Geol 200:1–9

Malet J-P, Remaître A, Maquaire O, Ancey C, Locat J (2003) Flow susceptibility of heterogeneous marly formations. Implications for torrent hazard control in the Barcelonnette basin (Alpes-de-Haute-Provence, France), *in* D. Rickenmann & C.-L. (Eds) Chen, ed., 'Third International Conference on Debris-Flow Hazard Mitigation: Mechanics, Prediction and Assessment', Millpress, Rotterdam, Davos, Switzerland, 351–362

Malet J-P, Maquaire O, Remaître A (2004) Assessing debris flow hazards associated with slow moving landslides: methodology and numerical analyses. Landslides 1:83–90

Malet J-P, Laigle D, Remaître A, Maquaire O (2005) Triggering conditions and mobility of debris flows associated to complex earthflows. Geomorphology 66:215–235

Maquaire O, Malet J-P, Remaître A, Locat J, Klotz S, Guillon J (2003) Instability conditions of marly hillslopes: towards landsliding or gullying? The case of the Barcelonnette basin, South East France. Eng Geol 70(1–2):109–130

Mitchell JK (1993) Fundamentals of soil behavior, second edition, Wiley

Ovarlez G, Mahaut F, Deboeuf S, Lenoir N, Hormozi S, Chateau X (2015) Flows of suspensions of particles in yield stress fluids. J Rheol 59(6):1449–1486

Picarelli L, Urciuoli G, Russo C (2004) Effect of groundwater regime on the behaviour of clayey slopes. Can Geotech J 41(3):467–484

Picarelli L, Urciuoli G, Ramondini M, Comegna L (2005) Main features of mudslides in tectonised highly fissured clay shales. Landslides 2(1):15–30

Renalier F, Bièvre G, Jongmans D, Campillo M, Bard PY, Miller RD, Bradford JH, Holliger K, ed. (2010) Clayey landslide investigations using active and passive VS measurements, Vol. 15, Advances in Near-Surface Seismology and Ground-Penetrating Radar, Geophysical Dev. Series

Rickenmann D, Laigle D, McArdell BW, Hubl J (2006) Comparison of 2D debris-flow simulation models with field events. Comput Geosci 10:241–264

Santamarina JC, Klein KA, Wang YH, Prencke E (2002) Specific surface: determination and relevance. Can Geotech J 39:233–241

Sridharan A, Prakash K (2000) Percussion and cone methods of determining the liquid limit of soils: controlling mechanisms. Geotech Test J 23:236–244

Trulsson M, Bouzid M, Kurchan J, Clément E, Claudin P, Andreotti B (2015) Athermal analogue of sheared dense Brownian suspensions. Europhys Lett 111:18001

van Asch TWJ, Malet J-P (2009) Flow-type failures in fine-grained soils: an important aspect in landslide hazard analysis. Nat Hazards Earth Syst Sci 9(5):1703–1711

Yukselen Y, Kaya A (2006) Prediction of cation exchange capacity from soil index properties. Clay Miner 41:827–837

Electronic supplementary material The online version of this article (https://doi.org/10.1007/s10346-018-0972-6) contains supplementary material, which is available to authorized users.

S. R. Carrière (✉) · D. Jongmans · G. Bièvre · B. Lanson
CNRS, ISTerre,
Université Grenoble Alpes,
38000, Grenoble, France
Email: simon.carriere@hotmail.fr

G. Chambon
IRSTEA, UR ETGR,
Université Grenoble Alpes,
Grenoble, France

L. Bertello · M. Berti
Dipartimento di Scienze Biologiche, Geologiche e Ambientali,
Universita' di Bologna,
40127, Bologna, Italy

M. Jaboyedoff (✉)
Université de Lausanne,
Géopolis, Switzerland
Email: michel.jaboyedoff@unil.ch

J.-P. Malet
Institut de Physique du Globe de Strasbourg,
CNRS UMR 7516 / Université de Strasbourg,
5 rue Descartes, 67084, Strasbourg Cedex, France

J. E. Chambers
British Geological Survey,
Keyworth, UK